Environmental Earth Sciences (2018) 77:318
https://doi.org/10.1007/s12665-018-7500-9

THEMATIC ISSUE

Riverbank filtration in Cairo, Egypt: part II—detailed investigation of a new riverbank filtration site with a focus on manganese

S. Paufler[1] · T. Grischek[1] · R. Bartak[1] · K. Ghodeif[2,3] · R. Wahaab[3] · H. Boernick[4]

Received: 1 October 2017 / Accepted: 16 April 2018 / Published online: 21 April 2018

Abstract

A 5-day detailed field investigation at a new RBF test well gallery in Embaba, Cairo, was conducted to evaluate the hydraulic setting and the behavior of iron and manganese. The well gallery consists of six vertical wells placed along a straight line parallel to the Nile riverbank. A low anisotropy factor for the aquifer ($k_{f,h}$:$k_{f,v}$) of 1.7 was determined by evaluation of a multi-step pumping test. Travel times between 11 days from the river toward the central wells and 22 days toward the outermost wells were estimated by groundwater flow modeling and particle tracking. The riverbed is rich in fine suspended sediments that have elevated iron and nitrogen concentrations. Depth-dependent water sampling during regular well operation indicates that the thick organic-, Fe- and Mn-rich riverbed is the primary source for ammonium, iron and manganese in the bank filtrate. Iron-rich groundwater flow from the opposite riverbank was identified as a secondary source of iron in the pumped water. The vertical position of the filter screen affects total travel times but would not reduce the portion of Mn-rich bank filtrate. The authors recommend continuous well operation for achieving stable water quality and lowering the risk of well clogging.

Keywords Riverbank filtration · Manganese · Depth-dependent sampling · Nile River · Egypt

Introduction

Rapid economic development and population growth lead to an increasing water demand in many countries. The global water demand is projected to increase by 55% in 2050 and causing severe water stress, e.g., in North and South Africa (WWAP 2016). Egypt faces already a water shortage of around 13.5 billion cubic meters per year (BCM/year), that is expected to continuously increase up to 26 BCM/year in 2025 (Omar and Moussa 2016). Currently, this shortage can be compensated by drainage reuse, which consequently deteriorates the water quality. Riverbank filtration (RBF) has been successfully used as natural and cost-efficient water treatment in many countries in Europe (e.g., Bourg and Bertin 1993; Grischek et al. 2002), the USA (e.g., Ray et al. 2003; Regnery et al. 2015) and Asia (e.g., Sandhu et al. 2011; Suratman et al. 2014).

Ghodeif et al. (2016) showed the potential for application of RBF along the Nile River in Egypt. The water demand of the Egyptian capital Cairo is mainly met by abstraction of surface water from the Nile River and subsequent treatment using flocculation, filtration and disinfection. One of the largest waterworks is located in Embaba, Cairo, with a total capacity of 1.2 million m^3 per day. To cope with the increasing water demand, the Holding Company for Water and Wastewater (HCWW) plans to expand the capacity of the waterworks Embaba (Fig. 1). The potential RBF site was first assessed in 2012 during a 3-day field investigation (Bartak et al. 2014). Groundwater, Nile river water and riverbed sediment samples indicated unfavorable conditions for the application of RBF.

This article is part of a Topical Collection in Environmental Earth Sciences on "NovCare—Novel Methods for Subsurface Characterization and Monitoring: From Theory to Practice," guest edited by Uta Sauer and Peter Dietrich.

Electronic supplementary material The online version of this article (https://doi.org/10.1007/s12665-018-7500-9) contains supplementary material, which is available to authorized users.

✉ S. Paufler
sebastian.paufler@htw-dresden.de

1 Dresden University of Applied Sciences, Friedrich-List-Platz 1, 01069 Dresden, Germany

2 Suez Canal University, 4.5 km The Ring Rd., Ismailia, Egypt

3 Holding Company for Water and Wastewater, Corniche El-Nile, Rod El-Farag, Cairo, Egypt

4 Institute for Water Chemistry, TU Dresden, Bergstr. 66, 01062 Dresden, Germany

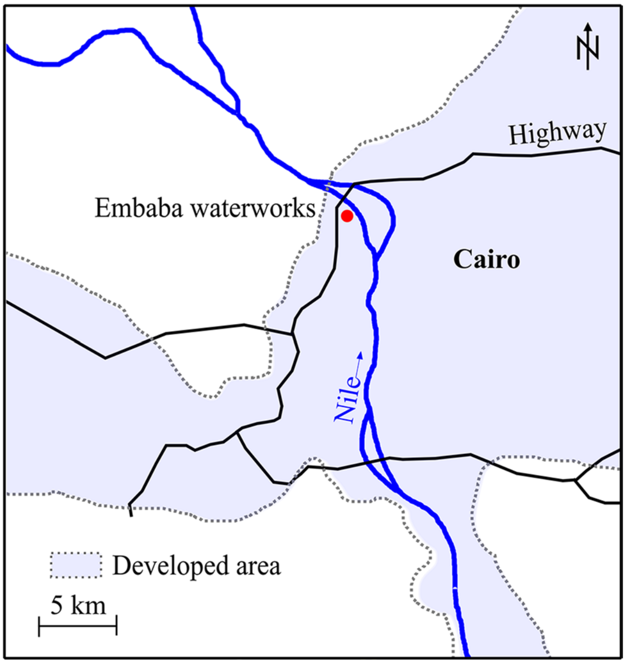

Fig. 1 Location of Embaba waterworks

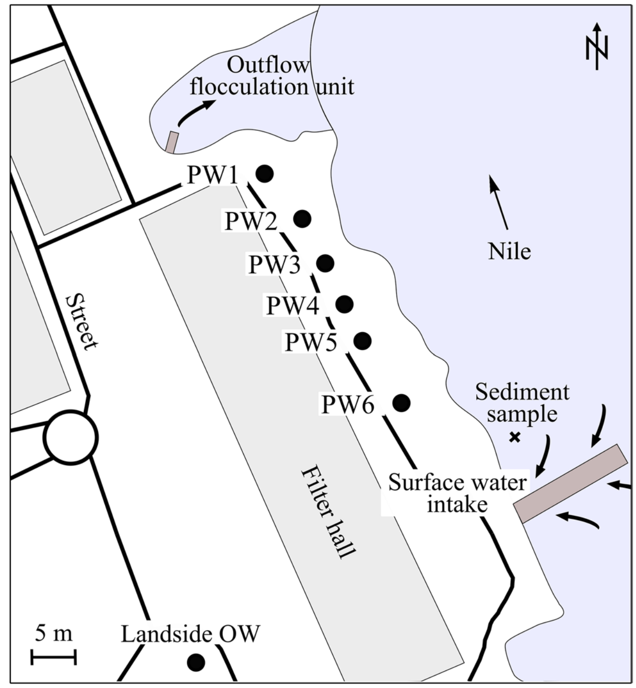

Fig. 2 Top view of the study area

In particular, sedimentation behind the surface water intake was suspected to foster severe clogging in front of the planned catchment. Since riverbed clogging usually causes water quality as well as water quantity issues during RBF (Schubert 2002; Ulrich et al. 2015; Grischek and Bartak 2016; Przybyłek et al. 2017), a more detailed investigation of the feasibility of RBF in Embaba was necessary and the construction of a test well was proposed. In 2015, six pumping wells (PW) were drilled to assess the applicability of RBF at the site (Fig. 2). Details and first monitoring results are presented in Ghodeif et al. (2018).

The aim of this paper is to show an approach to assess the suitability of RBF within a limited time frame and available equipment. Consequently, this paper highlights the results from a 5-day detailed field investigation including a pumping test and depth-dependent water sampling in pumping wells during operation. Based on the field results, a simplified groundwater flow model was built that helped to evaluate the suitability of the site conditions for RBF. Finally, suggestions are given for the improvement of the test site to achieve full-scale RBF application in Embaba.

Materials and methods

Riverbed sediment analysis

Five sediment samples were taken from the clogging layer of the Nile riverbed in front of the RBF wells (Fig. 2), mixed for analysis, sieved to gain the fraction < 2 mm and air-dried. Total Kjeldahl nitrogen (TKN) was determined according to DIN EN 16169. Total organic carbon (TOC) was measured after DIN EN 13137. Furthermore, samples were analyzed for heavy metals such as As, Cd, Cr, Cu, Fe, Mn, Ni, Pb and Zn according to DIN EN ISO 11885 and Hg according to DIN EN ISO 12846. Analyses were conducted by the laboratory Ergo Umweltinstitut GmbH (DIN EN ISO/IEC 1705 certified).

Regular monitoring of raw water quality

After the six pumping wells went in operation in July 2015, multiple samples from all PW were taken by the laboratory of the HCWW. Samples were analyzed in the laboratory for electrical conductivity (EC), pH, turbidity, alkalinity, major cations and anions, iron (Fe), manganese (Mn), ammonium (NH_4^+) and total organic carbon (TOC). Details are described in Ghodeif et al. (2018).

At various RBF sites, persistent micropollutants like pesticides, pharmaceuticals and sweeteners in river water and bank filtrate were used as tracer or to determine the portion of bank filtrate in the pumped water (e.g., Grischek et al. 1997; Heberer et al. 2004; Massmann et al. 2008a, b). In order to check the applicability of such an approach in Embaba, one water sample was screened for > 50 organic micropollutants.

Depth-dependent water sampling and temperature measurement

Water samples from PW were taken regularly by HCWW from the standpipe above the surface. Thus, each water sample represents a composite of bank filtrate and groundwater entering the 24 m long screen. Depth-dependent sampling makes it possible to determine whether discrete zones along the filter screen show varying water qualities. Common depth-dependent sampling approaches first remove the pump and afterward lower a smaller pump combined with a packer system.

Several authors used an efficient method to collect depth-dependent water samples with a small diameter hose and additional flow rate logging during well operation (e.g., Izbicki et al. 1999; Landon et al. 2010). This avoids time-consuming removal of the pump and makes expensive equipment unnecessary. The more important advantage is that steady-state flow conditions to the well are not disturbed by removing the pump.

For depth-dependent sampling in Embaba, a peristaltic pump (Model 410, Solinst Ltd, Canada) with an attached 3×0.5 mm PTFE hose was used. Using a suction pump located at ground level includes the limitation to about 8 m max drawdown below ground level in a well. As additional weight for lowering the hose beneath the pump and to avoid large particles entering the hose, a metal sinter filter (pore size 200 µm) was fitted to the hose end. The hose was lowered through the inner observation well (OW) and past the pump inside the well casing. Water was sampled every 5 m from the bottom of the well to the top of the filter screen. At least 1.5 hose volumes were pumped before sampling. EC was measured on-site for each sample (3430i, WTW Weilheim, Germany). Water samples were filtered on-site through 0.45 µm membrane filters. Major cations K^+, Na^+, Ca^{2+}, Mg^{2+} and dissolved heavy metals such as As, Cd, Cr, Cu, Fe, Mn, Ni and Zn were measured with ICP-OES (Optima 4300 DV, PerkinElmer, Waltham, MA, USA). Br^-, Cl^-, F^-, NO_2^-, NO_3^-, PO_4^{3-} and SO_4^{2-} were determined with ion-chromatography (autosampler AS50, eluent generator EG50, gradient pump GP50, electrochemical detector ED50, separation column AS19, all from Dionex). Organic micropollutants were analyzed by LC–MS/MS (LC: 1100 Agilent, MS detector: Q3200, AB Sciex) after filtration (membrane filter, pore size 0.45 µm) and enrichment (solid phase extraction using SiliaPrepX® HLB, 200 mg, 3 ml, from SiliCycle, enrichment factor 500) at the Institute for Water Chemistry, TU Dresden, Germany.

Because no flow rate data logs were available for the pumping wells, reliability of the measurements was checked by mixing calculations. Manganese concentration profiles of groundwater flowing toward the wells were calculated based on the measured Mn profiles from PW3 and PW6 for four possible flow distributions (Eq. 1). Calculations started at the lower filter screen edge, where the flow inside the well at a certain point is the sum of inflow from all points deeper in the well. Since no mixing with deeper groundwater was assumed to occur at the lowest point, the measured Mn concentration in the well reflected the aquifer concentration (Sukop 2000). The effect of mixing with groundwater through the lifting of the hose is taken into account by Eq. 1.

$$c_{\mathrm{Aq},n} = \frac{c_{\mathrm{well},n} * \sum_{i=1}^{n} Q_i - \sum_{i=1}^{n-1} \left(Q_i * c_{\mathrm{Aq},i}\right)}{Q_n} \tag{1}$$

c_{Aq}, calculated Mn concentration of groundwater in the aquifer in mg/l; c_{well}, measured Mn concentration along the filter screen inside the well in mg/l; Q, estimated flow rate towards the well in m^3/h.

Estimation of aquifer properties and travel time

A multi-step pumping test was carried out to estimate aquifer properties. To re-establish natural flow conditions, all six wells were switched-off 24 h in advance to the pumping test. Because of missing observation wells, the PW were sequentially switched-on and the remaining wells functioned as observation wells (Table 1). Water levels were manually monitored with an electric contact meter and with automatic pressure loggers (Mini Diver, Van Essen Instruments B.V., Delft, The Netherlands). PW5 and subsequently PW4 were switched-on after drawdown in the OW's was constant (±0.01 m) for at least 15 min.

Table 1 Well operation during the multi-step pumping test

Step	Well no.					
	PW1	PW2	PW3	PW4	PW5	PW6
Initial	All wells switched-off 24 h before starting the first well					
1	Not used	Monitoring	Monitoring	Monitoring	Monitoring	Pumping
2	Not used	Monitoring	Monitoring	Monitoring	Pumping	Pumping
3	Not used	Monitoring	Monitoring	Pumping	Pumping	Pumping

Evaluation of the pumping test was carried out using the software AQTESOLV (Duffield 2007). To estimate vertical anisotropy of the aquifer ($k_{f,h}$:$k_{f,v}$), the Neuman solution (Neuman 1974) for unconfined aquifers was chosen. The hydraulic conductivity of the aquifer ($k_{f,h}$) of 5×10^{-4} m/s (43.2 m/day) was taken from Ghodeif et al. (2018) and aquifer geometry (Online Resource 1) was adopted from Bartak et al. (2014).

Based on discharge measurements and known saturated aquifer thickness of ≈ 50 m, transmissivity (T) was fixed at 0.025 m^2/s and $k_{f,h}$:$k_{f,v}$ was variable. A constant head boundary represented the Nile River. Since AQTESOLV has no option to implement a third-type boundary (Cauchy), the so-called characteristic leakage length (Eq. 2) was used to move the boundary by a virtual distance away from the well (Haitjema et al. 2001). The characteristic leakage length represents a virtual flow distance within the aquifer on which the head loss would be equal to the actual head loss by the clogging layer.

$$\lambda = \sqrt{\frac{k_{f,h} * H * M}{k_{f,clog}}} \tag{2}$$

λ, characteristic leakage length in m; $k_{f,h}$, horizontal hydraulic conductivity of the aquifer in m/s; $k_{f,clog}$, hydraulic conductivity of clogging layer in m/s; M, thickness of clogging layer in m; H, saturated aquifer thickness in m.

Hydraulic conductivity of the clogging layer ($k_{f,clog}$) and subsequently total travel times (t_A) from the river to the wells were estimated by groundwater flow and transport modeling using Modflow-2005 code (Harbaugh 2005) with Model Muse (Winston 2009). The model domain covered an area of 2200 m × 1900 m. Mesh size was 1 m around the pumping wells and increased (factor ≤ 1.2) to maximum 10 m at the model boundaries (Fig. 3). Slope of the Nile river was set to 0‰. The real slope is estimated to be 0.02‰ (Ghodeif et al. 2018) which is very low and therefore neglected for modeling. To implement the actual depth of the 24 m long filter screen, the 60 m thick aquifer was divided into four layers (Fig. 4). For better implementation of vertical aquifer anisotropy in Model Muse, Layer 2 consisted of ten equally distributed sublayers.

Northern and southern model boundaries were no flow boundaries (Neumann BC). A constant head (CHB, Dirichlet BC) across all layers at the northeastern riverbank represented the groundwater level at the opposite riverbank. This prevented that the river boundary (Cauchy BC) acted as only possible water source. Along the western model boundary, a general head boundary (GHB, Cauchy BC) represented the unaffected groundwater level. The unaffected groundwater level was set to 16.6 m asl at a distance of 2500 m and

Fig. 3 Discretization of the catchment area and initial hydraulic heads without pumping

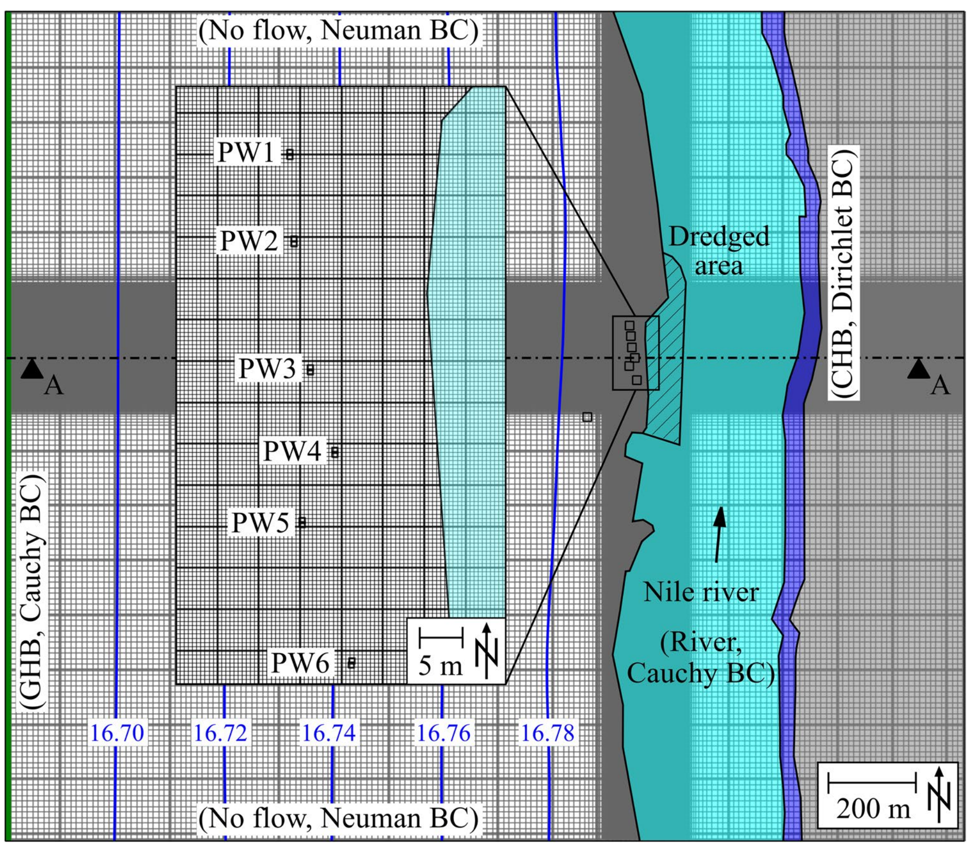

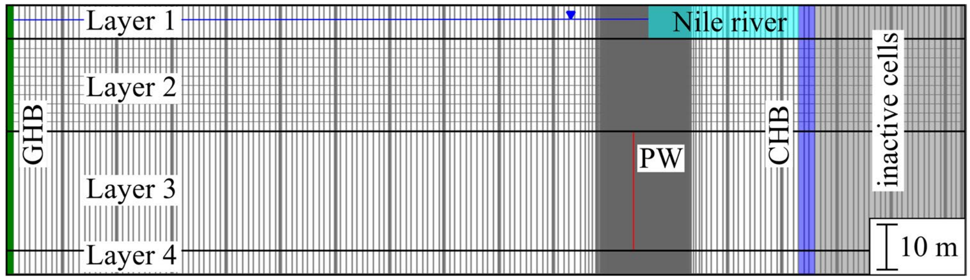

Fig. 4 Cross section A–A and vertical discretization of the catchment area without pumping

reflects the natural groundwater slope of around 0.083‰ (Ghodeif et al. 2018). Hydraulic conductance (C_b) of the GHB was calculated according to Eq. 3.

$$C_b = \frac{k_{f,h} * A}{l} \tag{3}$$

C_b, conductance of the GHB in m^2/s; A, area of river cell (A = length × width) in m^2; l, distance to the boundary in m.

Pumping test data were used for trial-and-error model calibration. Drawdown from initial water levels in the wells was set as calibration value because of missing accurate elevation data for absolute head measurements. Initial water levels were measured after 24 h without pumping. Time-steps 1, 2 and 3 had 4, 3 and 2 observation values for calibration. The pumping rate for each well was set to 4080 m^3/day and is the maximum pumping rate of the actual wells. Aquifer hydraulic conductivity remained constant at 5×10^{-4} m/s (43.2 m/day) during calibration. Hydraulic conductance of the Nile riverbed (CRIV) was used as calibration parameter (Eq. 4). All given CRIV in this publication refer to the cell area of 1 m^2 in front of the wells and are equal to the widely used leakage coefficient (Eq. 5). CRIV for cells with an area > 1 m^2 was automatically adjusted according to the different cell areas.

$$\mathrm{CRIV} = \frac{k_{f,clog} * A}{M} \tag{4}$$

CRIV, hydraulic conductance riverbed in m^2/s; A, area of river cell (A = length × width) in m^2

$$L = \frac{k_{f,clog}}{M} \tag{5}$$

L, leakage coefficient s^{-1}.

The initial CRIV of 2.5×10^{-4} m^2/s (21.6 m^2/day) was changed to 1.9×10^{-6} m^2/s (0.162 m^2/day) for best-fit calibration (trial-and-error). Root-mean-square-error (RMSE, Eq. 6) was chosen as indicator for best-fit. Calibration target was RMSE ≤ 0.1 m.

$$\mathrm{RMSE} = \sqrt{\frac{1}{n}\sum_{i=1}^{n}\left(s_{obs} - s_{sim}\right)_i^2} \tag{6}$$

RMSE, root-mean-square-error in m; s_{obs}, observed drawdown in m; s_{sim}, simulated drawdown in m; n, number of measurements.

The defined anisotropy factor of 5 for the aquifer and CRIV for the riverbed were assigned to the model for following travel time estimation using backward particle tracking with PMPath (Chiang and Kinzelbach 2001). Initial particle placement at each well was at the top, the middle and the bottom of the filter screen. Pumping rates for each of the six wells were set to the designed discharge of 3600 m^3/day. The impact of different clogging conditions was assessed in four scenarios for a 0.2 m thick clogging layer:

(a) Calibrated model.
(b) "Worst-case" clogging, $k_{f,clog} = 1 \times 10^{-7}$ m/s, CRIV = 0.043 m^2/day.
(c) Calibrated CRIV-value + removing clogging layer in front of the catchment.
(d) "Worst-case" status + removing clogging layer in front of the catchment.

The assumed clogging layer thickness of 0.2 m represents the mean clogging depth of 0.03 m for sand and 0.3 m for gravel at the Elbe river in Dresden (Beyer and Banscher 1976). Scenarios c and d were taken into account because a dredging vessel is regularly removing mud in front of the surface water intake from the riverbed (Fig. 2). Scenarios c and d assumed that after removal (dredging), a 0.02 m thin clogging layer remained on top of the aquifer, that had the $k_{f,clog}$ of the calibrated clogging layer (5×10^{-6} m/s). Thus, a CRIV of 21.6 m^2/day was assigned in the area in front of the catchment where the clogging layer was removed.

Heavy riverbed clogging can lead to an expansion of the cone of depression from the RBF wells up to the opposite riverbank (e.g., Przybyłek et al. 2017). In order to avoid the possible flow from groundwater from the opposite riverbank in Embaba, raising the deep filter screen was tested with the flow model. The filter screen position was changed from originally −9.5 to −33.5 m asl (24 m long) to 2.5 to −3 m asl with a length of 5.5 m (Online Resource 2). For raising the filter screen to 2.5 to −3 m asl in the flow model, the abstraction rate of each well (3600 m^3/day) was evenly distributed to three sublayers in layer 2. To check for possible modeling errors, abstraction was simulated using a CHB that represented the lowered water level in the wells during pumping. Additionally, the impact of an anisotropy factor of 10 for the aquifer to the raw water composition was tested.

Results

Nitrogen, carbon and heavy metal content of Nile clogging layer in Cairo

The mixed sample from the clogging layer of the Nile riverbed had a TKN content of 1100 mg/kg and a TOC content of 5600 mg/kg. Fe and Mn contents were 10,100 and 367 mg/kg. The content of As was low with < 3 mg/kg. Cd and Hg contents were < 0.3, Cr 12 and Cu 16.3 mg/kg. Contents of Ni, Pb, and Zn were 25, 6.17 and 26.7 mg/kg, respectively.

Quality of bank filtrate

Values for Fe and Mn determined in pumped water in Nov 2016 were 0.24–0.82 and 0.67–1.15 mg/l (Table 2) and are in good agreement with those observed by Ghodeif et al. (2018) from July 2015 to Nov 2016 (0.1–0.8 Fe and 0.4–1.1 mg/l Mn). Water from PW1 to 4 showed the highest Mn concentration with 1.02–1.15 mg/l. Water of PW6 had the lowest EC (408 µS/cm) among all wells. DOC and UV-absorbance at a wavelength of 254 nm showed a decrease by about 40% as a result of mixing, biodegradation and sorption processes in the aquifer. Chloride and sulfate concentrations are lower in the pumped water than in river water, indicating a significant portion of groundwater having lower concentrations. There are no problems with heavy metals in river water and bank filtrate.

In Germany, measurements of persistent micropollutants including pesticides, pharmaceuticals and sweeteners in river water and bank filtrate are used at various RBF sites to determine the portion of bank filtrate in the pumped water. Whereas for such calculation several sampling campaigns are required, especially regular river water quality monitoring, only random sampling was done in Embaba in Sept 2016 to check if this approach could be applied here too. A long list of micropollutants including acesulfame, 4-DMA-antipyrine, 4-IP-antipyrine, acetamipride, ametryn, amidotrizoate, atenolol, atrazine, benzotriazole, desethylatrazine, desisopropylatrazine, bentazone, bezafibrate, carbamazepine, carbofuran, ciprofloxacin, clothianidin, diazepam, diclofenac, diuron, gabapentin, glyphosate, hexazinone, iomeprol, iopamidol, isoproturon, linuron, loratadine, metformin, metoprolol, *N*,*N*-dimethylsulfamide, naproxen, paracetamol, phenazone, primidone,

Table 2 Water quality data for the Nile river and in PWs, Nov 9, 2016 ($n = 1$)

Parameter	Unit	Nile	PW1	PW2	PW3	PW4	PW5	PW6
EC	µS/cm	456	475	454	476	532	446	408
DOC[a]	mg/l	4.8	2.7	n.a.	2.8	2.7	3.1	n.a.
UV-254[a]	m^{-1}	8.0	4.6	n.a.	5.2	4.7	5.1	n.a.
Fe_{tot}	mg/l	0.07	0.69	0.82	0.43	0.58	0.48	0.24
Mn	mg/l	0.01	1.15	1.02	1.05	1.13	0.91	0.67
NH_4^+	mg/l	0.16	n.a.	n.a.	n.a.	n.a.	n.a.	2.16
Ca^{2+}	mg/l	32.0	41.0	40.5	42.0	47.2	39.5	35.9
Mg^{2+}	mg/l	14.9	14.7	13.9	15.3	16.9	13.8	12.9
Na^+	mg/l	43.6	34.5	29.8	31.3	35.9	32.0	30.2
K^+	mg/l	5.5	5.4	5.8	5.8	6.1	5.4	5.0
Cl^-	mg/l	34.1	24.4	22.6	24.3	26.9	21.1	20.5
SO_4^{2-}	mg/l	35.6	19.6	21.0	31.4	52.0	25.8	23.8
NO_3^-	mg/l	< 1	< 1	< 1	< 1	< 1	< 1	< 1
Br^-	mg/l	0.07	0.14	0.10	0.09	0.08	0.06	0.06
PO_4^{3-}	mg/l	n.a.	0.11	0.07	0.12	0.05	n.a.	0.08
As	mg/l	< 0.01	< 0.01	< 0.01	0.01	< 0.01	< 0.01	0.013
Cd	mg/l	< 0.003	< 0.003	< 0.003	< 0.003	< 0.003	< 0.003	< 0.003
Cr	mg/l	0.006	0.006	0.007	0.007	0.006	0.007	0.007
Cu	mg/l	0.023	0.022	0.022	0.022	0.022	0.022	0.022
Ni	mg/l	< .0.01	< 0.01	< 0.01	< 0.01	< 0.01	< 0.01	< 0.01
Pb	mg/l	< 0.01	< 0.01	< 0.01	< 0.01	< 0.01	< 0.01	< 0.01
Zn	mg/l	0.013	0.124	0.034	0.006	< 0.006	< 0.006	< 0.006

n.a. not analyzed

[a]Sampling on Sept 27, 2016

propanil, ranitidine, simazine, sulfamethoxazole, terbutryn and tolytriazole was found below the limit of quantification (LOQ) of 2–20 ng/l. Table 3 documents all micropollutants with concentrations found above the limit of detection (LOD) or around. In general, only very low micropollutant concentrations were found in Nile river water compared to major European rivers, probably due to limited industrial effluents and high discharge (mixing) and high temperature and bioactivity in the Nile River. Except for ibuprofen, all measured concentrations in river water were below the proposed safety threshold value of 100 ng/l for micropollutants in surface water used for drinking water supply. Ibuprofen was the only compound found with concentrations similar to those found in German rivers with significant input of sewage. The higher value in PW3 could be a result of a higher concentration in the river water a few weeks before sampling and different bank filtrate portion and travel times compared to the other PWs. The biodegradable caffeine is mostly removed during RBF. The quite persistent X-ray contrasting agents such as iomeprol, iohexol and iopromide show very low concentrations in river water and lower concentrations in bank filtrate, indicating mixing with non-polluted groundwater. Also, sweeteners as aspartame, cyclamate and saccharin were detected but at very low concentrations. Determination of organic micropollutants may not be applied at Embaba to calculate mixing of bank filtrate and groundwater because the concentration level in the Nile River is very low.

Fe and Mn distribution along the filter screens of PW3 and PW6

Depth-dependent water samples were taken every 5 m from the bottom to the estimated top of the filter screen. The sampling procedure was applied only at PW3 and PW6. PW3 represents the central part in the row of operated wells, where the highest drawdown and shortest travel times of bank filtrate were expected. Because PW6 is the southernmost well, lower drawdown and longer travel times from the river to the well were expected. The required time for one profile was about 3 h.

For PW3 and PW6, manganese concentrations varied between 0.60 to 0.71 mg/l along the lower 20 m of the filter screen (Fig. 5). The iron concentration showed a sharp peak of around 0.5 mg/l at 5 m above the lower filter screen edge and decreased toward the upper screen section. Along the upper 5 m of the filter screen of PW3, iron and manganese concentrations increased to 0.45 and 0.97 mg/l, respectively. In PW6, manganese remained almost steady at 0.62–0.64 mg/l along the entire screen section.

The reliability of the measurements was checked by a mixing calculation (Fig. 6). If uniform inflow was assumed along the filter screen of PW3, a concentration of 2.1 mg/l was calculated at the top of the filter screen, which was double the measured concentration. A non-uniform inflow of 60, 70 and 80% within the upper half of the filter screen (− 19 to − 4 m asl) resulted in a concentration of 1.2–1.3 mg/l, which was close to the measured value of 1.0 mg/l. The inflow distribution had very little effect on the difference between measured and calculated concentration for the lower half of the filter screen. For PW6, no or very little effect was observed for the Mn concentration when a uniform or non-uniform inflow was applied (Online Resource 3). The mixing calculation was repeated for iron and showed similar qualitative and quantitative changes in the same order of magnitude (data not shown).

Estimated aquifer anisotropy and travel times

Pumping test data (Fig. 7) were analyzed with AQTESOLV to check the plausibility of the parameter set and the hydraulic connection of observation wells and used to estimate vertical anisotropy ($k_{f,h}$:$k_{f,v}$) of the aquifer (Table 4). Initial CRIV was set to 21.6 m^2/day and based on the assumption that $k_{f,clog}$ (5×10^{-5} m/s) is around 1/10 of hydraulic conductivity of the aquifer (5×10^{-4} m/s). Using Eq. 4 resulted in $\lambda = 10$ m, equal to the actual distance to the riverbank. The

Table 3 Organic micropollutants in ng/l in Nile River water and PWs, Sept 27, 2016 ($n = 1$)

Micropollutant	Source/use	Nile	PW1	PW3	PW4	PW5
Aspartame	Sweetener	16	< 2	7	3	< 2
Caffeine	Coffee	34	4	8	4	2
Cotinine	Tobacco	4	< 2	< 2	< 2	< 2
Cyclamate	Sweetener	0.6	0.4	0.2	0.4	0.4
Diuron	Herbicide	5.5	5.4	5.8	6.1	5.4
Ibuprofen	Pharmaceutical	60	45	154	38	49
Iohexol	X-ray contrast agent	3	2	2	3	5
Iopromide	X-ray contrast agent	4	< 2	< 2	< 2	< 2
Saccharin	Sweetener	2	1	1.2	0.4	0.4
Theophyllin	Tea, pharmaceutical, degradation product of caffeine	3	< 2	< 2	< 2	< 2

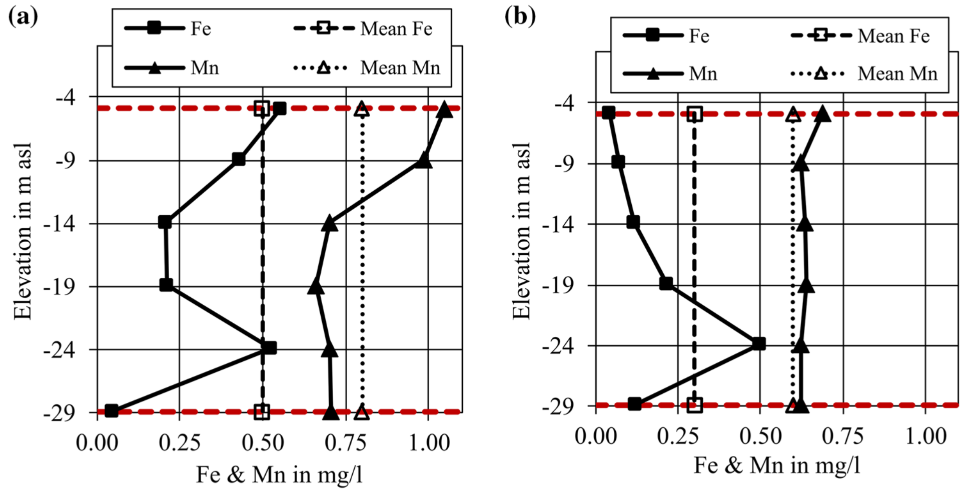

Fig. 5 Fe and Mn in **a** PW3 and **b** PW6 along the filter screen. Dashed red lines indicate the top and the bottom of the filter screen

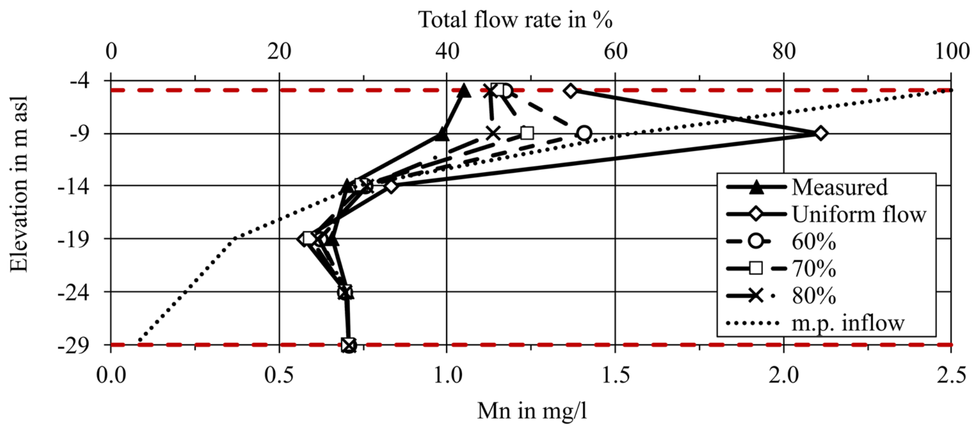

Fig. 6 Calculated Mn concentration in the aquifer from PW3 for uniform inflow, 60, 70 and 80% inflow at the upper half of the filter screen. Dashed lines indicate filter screen position. Dotted black line indicates the most probable inflow distribution after Tügel et al. (2016) for wells with long filter screens

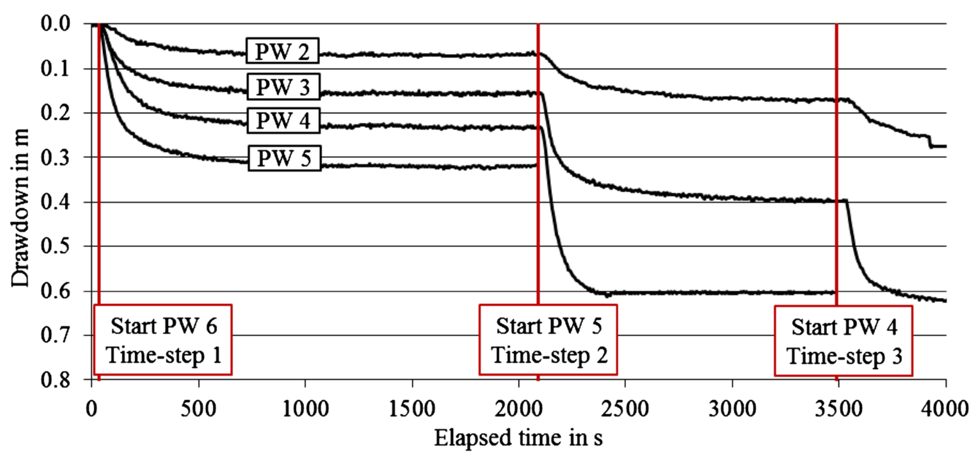

Fig. 7 Observed drawdown during the pumping test in PW5–PW2

initial estimation did not lead to convergence. Subsequently, CRIV was set to 2.16 m^2/day ($k_{f,clog} = 1/100\ k_{f,h}$) resulting in $\lambda = 32$ m and enabled auto estimation. Further increase in λ to 80 and 180 m was tested but had only minor effects to the matched results. The entire pumping test and all three time-steps were independently evaluated. Estimated aquifer anisotropy was 2.2 for evaluation of the entire pumping test as step-drawdown test. Auto estimation for independent evaluation of time-step 1, 2 and 3 resulted in anisotropies of 4.1, 2.0 and 1.3, respectively. Results indicated a very low porosity of 0.10 (mean, $n = 4$). Since it was assumed that the sandy aquifer is mostly unconfined, the actual porosity is

Table 4 Estimated aquifer anisotropy and porosity from AQTESOLV

Time-step	$k_{f,h}$:$k_{f,v}$	Porosity	Variance	Standard deviation
1 + 2 + 3	2.2	0.50	0.00487	0.06977
1	4.1	0.09	0.00009	0.00940
2	2.0	0.11	0.00469	0.06855
3	1.3	0.03	0.00166	0.04079
Median	1.7	0.10		

probably around 0.2–0.3. Because transmissivity was fixed, the Neumann solution underestimated anisotropy of the aquifer, too. Thus, for the subsequent modeling with Model Muse anisotropy of the aquifer was set to 5, as discussed later.

The initial CRIV of 21.6 day^{-1} ($k_{f,clog} = 5\times10^{-5}$ m/s) resulted in a RMSE of 0.17 m. Best-fit was achieved for a CRIV of 2.16 day^{-1} ($k_{f,clog} = 5\times10^{-6}$ m/s) with a RMSE of 0.12 m and applied in the model (Online Resource 4). The designed pumping rates of 3600 m^3/day were used for modeling scenarios because the maximum pumping rates could be only achieved as the water was directly discharged back to the river and not into the collecting main. CRIV varied according to scenarios a–d (Table 5).

Estimated total travel times for scenario a (calibrated model = 100%) resulted in travel times of 11–22 days (Table 4). For the worst-case clogging conditions (scenario b), travel times increased to 23 (209%) to 85 d (386%). After removing the clogging layer in front of the riverbank (scenarios c and d), travel times decreased by 13–27%. Travel times for scenarios c and d were equal. Compared to scenario a, the bank filtrate (BF) portion decreased to 43% when worst-case clogging was assumed (scenario b). Removing the clogging layer had only minor impact (< 1%) for calibrated clogging conditions (scenarios a-c) but led to an increase by 34.5% for worst-case clogging conditions (scenario b–d). For both worst-case scenarios b and d, the water budget showed that the wells abstracted 44 and 16% groundwater from the opposite riverbank flowing beneath the riverbed.

Discussion

Accuracy of the groundwater flow model

To estimate travel times between the Nile and the pumping wells and to test possible improvement options, a simplified groundwater flow model was set-up for Embaba. Evaluation of a pumping test with AQTESOLV gave an estimated anisotropy of 1.7 for the aquifer, which is low. A sensitivity analysis proved that a different aquifer anisotropy factor did not change the calibration in Model Muse substantially. Using $k_{f,h}$:$k_{f,v}$ of 5 and 10 changed the RMSE by only < 0.1% (data not shown). An anisotropy factor of 5 for the aquifer was selected and the middle range between the suggested value from AQTESOLV and the typical upper value of 10 for unconsolidated aquifers (Hölting and Coldewey 2013). Su et al. (2004) for example, determined an anisotropy factor of 5 for alluvial aquifer sediments.

Because of an almost vertical flow path from the Nile River to the well screens, a higher vertical aquifer anisotropy would have greatly prolonged the simulated travel times from the river to the wells. A lower effective porosity would have shortened simulated travel times. Due to a lack of data, a standard value of 25% for effective porosity was used in this study. Sefelnasr and Sherif (2014) reported a low effective porosity of 12–19% for the Nile delta aquifer north of Cairo. After Sherif (1999) an effective porosity of 30% is representative for the same study area. Thus, the applied value is within the reported span but near the upper limit. Although the divergent effects of a higher aquifer anisotropy and lower effective porosity might even out their individual effects on travel time, the absolute error cannot be exactly

Table 5 Shortest estimated travel times as a function of CRIV

Scenario	CRIV	$k_{f,clog}$	Travel time from the river to well no.						BF portion	GW portion	
			PW1	PW2	PW3	PW4	PW5	PW6		Landside	Beneath riverbed
	m^2/day	m/s	Days	Days	Days	Days	Days	Days	%	%	%
a	2.16	5×10^{-6}	22	14	12	11	15	16	91.5	5.0	3.5
	% of actual estimated t_A		100	100	100	100	100	100			
b	0.043	1×10^{-7}	85	29	24	23	39	50	43.0	13.0	44.0
	% of actual estimated t_A		386	207	200	209	260	313			
c	2.16	5×10^{-6}	16	12	10	9	13	13	92.5	4.5	3.0
	% of actual estimated t_A		73	86	83	82	87	81			
d	0.043	1×10^{-7}	16	12	10	9	13	13	77.5	6.5	16.0
	% of actual estimated t_A		73	86	83	82	87	81			

evaluated for the estimated travel times. Thus, it was decided to evaluate the travel times mostly qualitatively rather than quantitatively.

Transmissivity was fixed at 0.025 m^2/s during aquifer anisotropy estimation with AQTESOLV and for subsequent flow modeling. This value was based on the estimated saturated aquifer thickness of 50 m, and $k_{f,h}$ of the aquifer (5×10^{-4} m/s = 43.2 m/day), that Ghodeif et al. (2018) determined by sieve analysis. Bartak et al. (2014) used a transmissivity of 0.03 m^2/s for the same study site and Sefelnasr and Sherif (2014) reported a transmissivity of 0.023–0.035 m^2/s (2000–3000 m^2/day) for the Nile delta north of Cairo. Thus, the adopted T of 0.025 m^2/s is in good agreement with the reported data.

Best-fit for calibration was mainly a function of aquifer hydraulic conductivity and leakage factor. RMSE for the calibrated model was with 0.12 m slightly higher than the pre-set calibration target of 0.1 m. Because the major target of the flow model was supporting the first evaluation of the field site, rather than building a precise model of the catchment, the result of the trial-and-error calibration was accepted to be sufficiently accurate.

Evaluation of the existing RBF system

Iron and manganese concentrations of the pumped water at Embaba were similar to observations from other RBF sites worldwide. Iron concentrations of around 0.5 mg/l in Embaba are less than usually observed during RBF under anoxic conditions (e.g., Grischek et al. 1995; Massmann et al. 2004). The measured Mn concentrations of up to 1 mg/l are also common for many anoxic RBF sites (Grischek and Paufler 2017).

Riverbed sediments from the Nile river showed an elevated iron content with 10,100 mg/kg. Bartak et al. (2014) determined at the same study site up to 37,000 mg/kg Fe and 780 mg/kg Mn for the top layer of the riverbed as well as 11,000 mg/kg Fe and 130 mg/kg Mn for aquifer material (both grain size < 2 mm). Paufler (2015) measured Fe and Mn contents around 1000 and 250 mg/kg for riverbed sediments (grain size < 2 mm) from the Elbe river in Dresden, Germany. Grischek (2003) determined an iron content of 3500 mg/kg in aquifer material (grain size < 2 mm) from the alluvial aquifer in Torgau (Germany). The grain size fraction < 0.2 mm of riverbed sediments from the Glatt River in Switzerland contained 6700 mg/kg Fe and 280 mg/kg Mn (von Gunten et al. 1994). Bourg et al. (1989) determined up to 32,000 mg/kg Fe and 380 mg/kg Mn in riverbed sediments of the heavily polluted Deûle River, France. Reduction of Fe-/Mn(hydr)oxides is a common source for elevated Fe and Mn concentrations during RBF (e.g., Jacobs et al. 1988; Massmann et al. 2008a).

Results of the depth-dependent water sampling indicate different flow conditions toward some wells within the gallery. Fe and Mn concentration profiles in PW3 indicate that the wells in the center of the gallery receive iron- and manganese-rich water mainly via the upper part of the filter screen. This observation would suggest a possible reductive dissolution of the Fe/Mn(hydr)oxides within the riverbed. Furthermore, iron concentration profiles in PW3 and PW6 showed similar peaks at the lower edge of the filter screen. A possible explanation is that old, anoxic and iron-rich groundwater is flowing from the opposite riverbank beneath the riverbed toward the wells. Results from flow modeling show that a large portion of groundwater flow from the opposite riverbank can be expected in case of a heavily clogged riverbed. The current dredging scheme could be another explanation for the observed profiles. Mud from the Nile riverbed is currently only removed around the surface water intake. PW6 is located adjacent to the intake and close to the area where the mud has been removed (Fig. 2). Thus, dredging the iron-rich mud in front of PW6 partly removed the potential source for iron. More importantly, oxygen-rich Nile water can perhaps pass the thin, remaining clogging layer and enter the aquifer without complete reduction of O_2 levels. As a result, oxygen prevents extensive Fe/Mn(hydr) oxide reduction and bank filtrate entering the upper part of the filter screen of PW6 contained less iron. Since the mud showed no elevated manganese content, the described effect was less visible for the manganese profile.

Accompanying flow rate logging during depth-dependent sampling as per the method of Izbicki et al. (1999) would have helped for data interpretation, but was not possible. Mixing calculations underlined that the manganese-rich bank filtrate enters the upper part of the filter screens of both wells even at the most unlikely inflow distribution (Fig. 5). More reasonable estimations of 60–80% inflow through the upper half of the filter screen (Tügel et al. 2016) led to similar results. When typical flow conditions are taken into account along PW6, the resulting concentration profile further supported the hypothesis that the manganese-rich water enters the upper filter screen section. Because all calculated concentration profiles showed only minor deviations from the measured concentrations inside the well, all measured Fe and Mn profiles in PW3 and PW6 were considered sufficiently reliable to draw further conclusions.

The TKN content of 1100 mg/kg in Nile riverbed sediments is slightly elevated. David et al. (2011) determined up to 1800 mg/kg TKN in sediments of the Vène river (French), downstream of a sewage treatment plant (STP). Sediment samples from riverbanks adjacent to agricultural activities in Canada contained 2000–5900 mg/kg TKN (Frey et al. 2015). Gil et al. (2009) measured between 900 and 6800 mg/kg in sediments of the Han river in Seoul (Korea). The Han river was highly polluted due to upstream inputs of pollutant and wastewaters. The TKN content of the sediment column was reduced by 50–60% through partial dredging of the upper riverbed layer. Matisoff et al. (1981) observed an increasing NH_4^+ concentration with higher TKN content of the sediment. Thus, the slightly elevated NH_4^+ concentrations in all wells (Table 2) could result from mineralization of organic nitrogen compounds within the riverbed. Diffuse pollution by fertilizers or sewage cannot be ruled out but has not been proven yet. Potential NH_4^+ sources could be tested by isotope sampling and determination of δ^{15}/NH_4^+ or δ^{15}/NO_3^- ratios.

The TOC content of 0.56 weight-% is within a common order of magnitude for riverbed sediments and is in agreement with the former measured TOC content of 1.1 weight-% at the same study site (Bartak et al. 2014). Diem et al. (2013) measured organic carbon contents of up to 1.7 weight-% for fine sediments of an alpine riverbed in Switzerland. Bourg et al. (1989) measured around 9 weight-% organic matter (OM) in riverbed sediments in France. Massmann et al. (2008a) determined between 0.2 and almost 10 weight-% OM in lake-bottom sediments in Berlin.

Table 2 shows that almost the highest Fe and Mn concentrations were measured at the northern-most PW1 and that concentrations decrease toward PW6. PW1 is placed adjacent to the outflow of the flocculation unit (Fig. 2). Aluminum sulfate ($Al_2(SO_4)_3$) is used as flocculant for pretreatment of surface water in Embaba. Alum sludge usually has high heavy metal content (e.g., Sengupta and Shi 1992), but dissolution of the sludge and accompanying metal release are unlikely to occur within Nile river water, which is aerobic and has a pH of around 8. Thus, the sludge is not considered to be the direct source for Fe or Mn. Albrecht (1972) mentioned that alum sludge could result in soil clogging when it is disposed of on land. Thus, the disposed flocculation sludge could contribute to riverbed clogging in front of the wells.

Impact of different clogging conditions on the existing RBF system

The impact of variable CRIV on the total travel times was qualitatively evaluated to minimize uncertainties from estimated aquifer anisotropy and effective porosity. Scenario c represents a possible improvement of the current calibrated situation (scenario a) by removing mud from the riverbed in front of the wells. Mud removal by dredging can reduce the local infiltration resistance and enable higher abstraction rates. It may also reduce the total travel time and prevent anoxic conditions that can cause the release of heavy metals such as Fe and Mn. Scenario b represents worst-case clogging conditions, in which total travel times increased up to 386% compared to scenario a (= 100%). A comparison of results from scenario a with those from scenarios b and c suggests that the travel time through the clogging layer itself does significantly shorten or prolong the total travel time. Already a 50-fold less-conductive clogging layer with a thickness of 0.2 m prolongs the total travel times by at least 100% (12 days) up to 286% (63 days). Removal of the clogging layer in scenarios c and d led to similar travel times as the hydraulic properties of the underlying aquifer were similar in both scenarios. Bartak et al. (2014) mentioned that > 70% of the riverbed material has a grain size of < 0.125 mm and the hydraulic conductivity of the riverbed is most probably $\ll 1.5 \times 10^{-5}$ m/s ($\ll$1.3 m/day). Grischek and Bartak (2016) determined a leakage coefficient between approx. 1×10^{-6} and 1×10^{-7} s^{-1} (0.086 and 0.0086 day^{-1}) for the Elbe river in Dresden. Taking the estimated clogging layer thickness of 0.2 m from Embaba, this would be equal to a $k_{f,clog}$ of 2×10^{-7} to 2×10^{-8} m/s (0.017–0.0017 m/day). Pholkern et al. (2015) measured $k_{f,clog}$ values up to of 1×10^{-6} m/s (0.086 m/day) for the Ping river in Thailand. Thus, the applied CRIV of 2.16 m^2/day ($k_{f,clog} = 5 \times 10^{-6}$ m/s) for Embaba is an optimistic estimation. That means that the determined travel times from the river to the wells should be considered as minimum travel times. For a RBF site at the Rhine river in Germany (slope 0.18‰, flow velocity 1.0–1.4 m/s), heavy clogging of a riverbed stretch with riverbed hydraulic conductivities around 1×10^{-8} m/s was observed up to 80 m apart from the riverbank (Schubert 2002). Taking the low slope of the Nile river of 0.02‰ (Ghodeif et al. 2018) and the low flow velocity of 0.5–0.7 m/s (Bartak et al. 2014) into account, severe clogging across almost the entire stream width of the Nile river is likely to occur in Embaba.

Estimated BF portions reflected the influence of the riverbed hydraulic conductivity. The BF portion was variable because the assigned constant head at the opposite riverbank was an additional water source within the domain. Above a $k_{f,clog}$ of around 3×10^{-6} m/s (0.22 m/day), the BF portion was ≈ 90% (Fig. 8). A hydraulic conductivity of the clogging layer one order of magnitude lower led to a BF portion of < 50%. Adopting the observed clogging conditions from other RBF sites, the BF portion in Embaba is probably less than 60%. Groundwater flow from the opposite riverbank

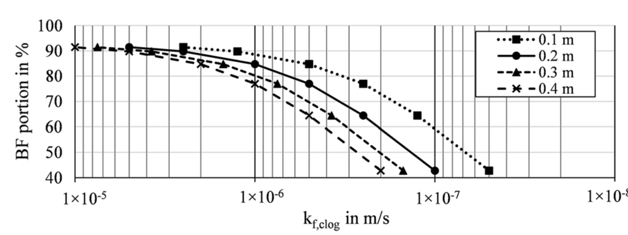

Fig. 8 Estimated portion of bank filtrate (BF) as a function of clogging layer thickness and hydraulic conductivity of the clogging layer

acting as another water source becomes even more likely when considering the deep filter screen position.

Potential improvements for future planning at the RBF site in Cairo

Due to a short distance between the Nile riverbank and the wells, an optimization of the filter depth could be beneficial to the existing RBF system. Even if RBF at Embaba occurs naturally, groundwater flow beneath the river contributing to elevated Fe concentrations cannot be ruled out. As shown in Fig. 8, riverbed clogging can result in BF portions < 50%.

Raising the elevation of the filter screen to 2.5 to − 3 m asl was tested in scenarios a–d as a means of increasing the BF portions. None of these simulated scenarios yielded a noteworthy increase in the BF portion (Fig. 9). To rule out modeling error being responsible for this result, the impact of two additional model approaches was tested. Modflow uses finite difference equations that do not recognize resistance between cells, if a well penetrates several layers. As a result, different heads are computed for each cell, although the head inside the well would be the average of the cells representing the well (Anderson 2005). Particle tracking indicated a preferential flow to the uppermost of the three cells (not shown). Applying a CHB that represented the lowered water level in each well simulated the total abstraction rate satisfactorily (20,870 m^3/day compared to 21,600 m^3/day total abstraction from six wells), but did not lead to different BF portions. The third approach tested an anisotropy factor of 10 for the aquifer, typical for unconsolidated aquifers (Hölting and Coldewey 2013). BF portions remained in the same ratio. Hence, elevating the filter screen to 2.5 to − 3 m asl is not useful to increase the BF portion in Embaba. Grischek (2003) similarly observed at two RBF sites along the Elbe River in Germany, that raising the filter screen position would not improve the raw water quality.

Due to the elevation of the filter screen, the estimated travel times from the river to the wells decreased by 35–83% (Fig. 10). The simulated reduction in travel time is probably distributed among the travel time within the clogging layer and the travel time through the underlying aquifer. Since the clogging layer is assumed to be the primary source for Fe and Mn, shorter travel times through the clogging layer could reduce the potential to release iron and manganese from the clogging layer. However, removal of organic pollutants, bacteria, viruses and parasites, and protection from shock loads would probably become less effective. Thus, if the estimated total travel times are in the correct order of magnitude, an elevation of the filter screen is not recommended for Embaba.

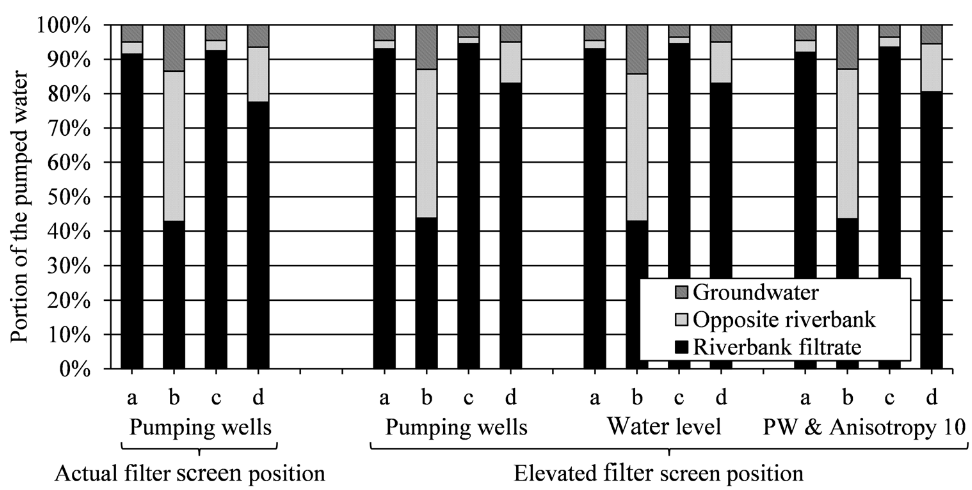

Fig. 9 Impact of an elevated filter screen position on the distribution of the different source waters. Scenarios a–d refer to different clogging conditions. See text for explanation

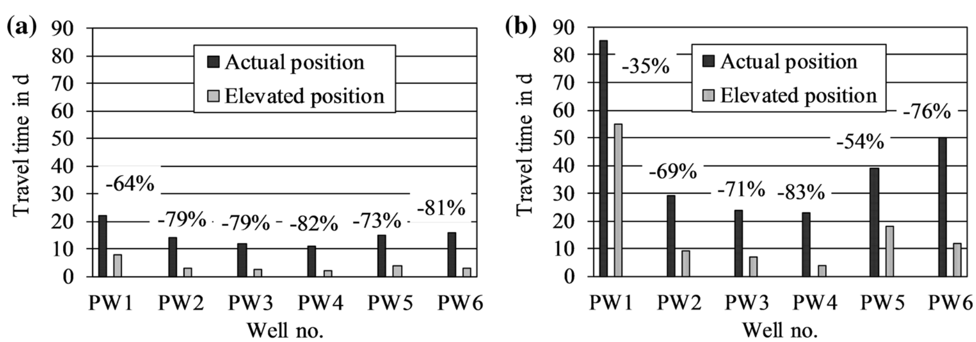

Fig. 10 Estimated reduction of travel times for **a** the calibrated clogging status and **b** worst-case clogging status with elevated filter screen from − 5 to − 29 m asl (current status) to 2.5 to − 3 m asl

Continuous well operation would have the beneficial effects of achieve stable water quality and lowering the risk of well clogging (sand input and iron incrustations). Furthermore, a decreasing total travel time and especially shorter residence time of the bank filtrate within the organic-, Fe- and Mn-rich riverbed would lead to lower concentrations of Fe and Mn in the pumped water. Grischek and Paufler (2017) showed for wells in Torgau and Dresden (Germany) that iron and manganese concentrations can decrease over longer time periods with continuous well operation.

Dredging the riverbed sediments in front of the entire riverbank instead of just around the surface water intake also has the potential to improve the quality of the bank filtrate. Gil et al. (2009) showed that dredging the upper sediment layer can reduce nutrient contents from the soil column by about 55%. Hence, removing the clogging layer in Embaba should lead to lower ammonium concentrations in the bank filtrate. Additionally, the results of the depth-dependent sampling showed that perhaps the removal of mud in front of PW6 led to a lower iron concentration in the bank filtrate.

Conclusions

A 5-day field investigation was conducted to evaluate the potential of a new RBF site in Cario, Egypt, with focus on the hydraulic setting and the behavior of iron and manganese. Minimum travel times between 11 days toward the central wells and 22 days toward the outermost wells were estimated by groundwater flow modeling and particle tracking. Riverbed sediments from the Nile river showed an elevated iron and nitrogen content. Depth-dependent water sampling during regular well operation showed that the thick organic-, Fe- and Mn-rich riverbed is the source for iron, manganese and ammonium in the bank filtrate. Removing the clogging layer using the available dredging vessel has the potential to improve the quality of the pumped water. The authors recommend testing the effect of entirely removing the clogging layer in front of the catchment. Additionally, iron profiles and flow modeling indicated an iron-rich groundwater flow beneath the river. Due to already short travel times from the river to the wells and only minor impact to the BF portion, elevating the deep filter screens would probably not improve water quality in Embaba. Continuous well operation would definitely be desirable and would have beneficial effects by achieving stable water quality and lowering the risk of well clogging.

Acknowledgements The latest investigations in this paper were performed as cooperation between the Holding Company for Water and Wastewater and the Division of Water Sciences at the University of Applied Sciences Dresden. The authors are grateful to the ESF for the financial support to S. Paufler (Grant No. 200031585) and to the German Science Centre and DAAD office in Cairo for promoting scientific collaboration.

References

Albrecht AE (1972) Disposal of Alum sludges. J Am Water Works Assoc 64(1):46–52

Bartak R, Grischek T, Herlitzius J (2014) Bank filtration under arid conditions for drinking water supply at low cost. Final report BMBF research project GEF10-186, FKZ 01DH12012A, 164p (**in German**)

Beyer W, Banscher E (1976) On the methodology for riverbank filtration site investigation. Z Angew Geol 22:149–154 **(In German)**

Bourg ACM, Bertin C (1993) Biogeochemical processes during the infiltration of river water into an alluvial aquifer. Environ Sci Technol 27(4):661–666

Bourg ACM, Darmendrail D, Ricour J (1989) Geochemical filtration of riverbank and migration of heavy metals between the Deûle river and the Ansereuilles alluvion-chalk Aquifer (Nord, France). Geoderma 44(2–3):229–244

Chiang WH, Kinzelbach W (2001) 3D-groundwater modeling with PMWIN, 1st edn. Springer, Berlin, p 346. ISBN 3540677445

David A, Perrin JL, Rosain D, Rodier C, Picot B, Tournoud MG (2011) Implication of two in-stream processes in the fate of nutrients discharged by sewage system into a temporary river. Environ Monit Assess 181(1–4):491–507. https://doi.org/10.1007/s10661-010-1844-2

Diem S, von Rohr RM, Hering JG, Kohler HP, Schirmer M, von Gunten U (2013) NOM degradation during river infiltration: effects of the climate variables temperature and discharge. Water Res 47(17):6585–6595

DIN EN 13137:2011-12 (2001) Characterization of waste—determination of total organic carbon (TOC) in waste, sludges and sediments. Beuth Verlag GmbH, Berlin

DIN EN 16169:2012-11 (2012) Sludge, treated biowaste and soil—determination of Kjeldahl nitrogen. Beuth Verlag GmbH, Berlin

DIN EN ISO 11885:2009-09 (2009) Water quality—determination of selected elements by inductively coupled plasma optical emission spectrometry (ICP-OES). Beuth Verlag GmbH, Berlin

DIN EN ISO 12846:2008-12 (2008) Water quality—determination of mercury: method using atomic absorption spectrometry (AAS) with and without enrichment. Beuth Verlag GmbH, Berlin

Duffield GM (2007) AQTESOLV for windows version 4.5 user's guide. HydroSOLVE, Inc., Reston

Frey SK, Gottschall N, Wilkes G, Grégoire DS, Topp E, Pintar KD, Sunohara M, Marti R, Lapen DR (2015) Rainfall-induced runoff from exposed streambed sediments: an important source of water pollution. J Environ Qual 44(1):236–247. https://doi.org/10.2134/jeq2014.03.0122

Ghodeif K, Grischek T, Bartak R, Wahaab R, Herlitzius J (2016) Potential of river bank filtration (RBF) in Egypt. Environ Earth Sci 75:671. https://doi.org/10.1007/s12665-016-5454-3

Ghodeif K, Paufler S, Grischek T, Wahaab R, Souaya E, Bakr M, Abogabal A (2018) Riverbank filtration in Cairo, Egypt—part I: installation of a new riverbank filtration site and first monitoring results. Environ Earth Sci 77(7):270. https://doi.org/10.1007/s12665-018-7450-2

Gil KI, Kim LH, Cho GC, Yoon J (2009) Evaluation of sediment contamination and effectiveness of dredging in mid-to-lower Han river. Water Air Soil Pollut 206(1):263–272. https://doi.org/10.1007/s11270-009-0103-z

Grischek T (2003) Management of bank filtration sites along the Elbe River. Dissertation, TU Dresden, Institute for Groundwater Management. ISSN 14300311, 252p (**in German**)

Grischek T, Bartak R (2016) Riverbed clogging and sustainability of riverbank filtration. Water 8(12):604. https://doi.org/10.3390/w8120604

Grischek T, Paufler S (2017) Prediction of iron release during riverbank filtration. Water 9(5):317. https://doi.org/10.3390/w9050317

Grischek T, Dehnert J, Nestler W, Neitzel P, Trettin R (1995) Groundwater flow and quality in an alluvial aquifer recharged from river bank infiltration, Torgau Basin, Germany. In: Brown AG (ed) Geomorphology and groundwater. Wiley, Hoboken, pp 21–35

Grischek T, Neitzel P, Andrusch T, Lagois U, Nestler W (1997) Behavior of EDTA during subsurface transport and identification of infiltration zones along the Elbe river. Vom Wasser 89:261–282 **(in German)**

Grischek T, Schoenheinz D, Worch E, Hiscock K (2002) Bank filtration in Europe—an overview of aquifer conditions and hydraulic controls. In: Dillon P (ed) Management of aquifer recharge for sustainability. Balkema Publ, Lisse, pp 485–488

Haitjema H, Kelson V, de Lange W (2001) Selecting MODFLOW cell sizes for accurate flow fields. Groundwater 39(6):931–938. https://doi.org/10.1111/j.1745-6584.2001.tb02481.x

Harbaugh AW (2005) MODFLOW–2005. The U.S. Geological Survey modular ground-water model—the ground-water flow process: U.S. Geological Survey Techniques and Methods 6–A16, 253p

Heberer T, Michelinski A, Fanck B, Knappe A, Massmann G, Pekdeger A, Fritz B (2004) Field studies on the fate and transport of pharmaceutical residues in bank filtration. Ground Water Monit Remediat 24:70–77. https://doi.org/10.1111/j.1745-6592.2004.tb00714.x

Hölting B, Coldewey WG (2013) Hydrogeologie. Einführung in die allgemeine und angewandte Hydrogeologie, 8th edn. Springer, Berlin, p 438 **(in German)**. ISBN 9783827423535

Izbicki JA, Christensen AH, Hanson RT (1999) U.S. Geological Survey combined well-bore flow and depth-dependent water sampler. USGS Fact Sheet 196-99, 2p. http://pubs.usgs.gov/fs/1999/fs19699/. Accessed 24 Jan 2017

Jacobs LA, von Gunten HR, Keil R, Kuslys M (1988) Geochemical changes along a river-groundwater infiltration flow path: Glattfelden, Switzerland. Geochim Cosmochim Acta 52(11):2693–2706

Landon MK, Jurgens BC, Katz BG, Eberts SM, Burow KR, Crandall CA (2010) Depth-dependent sampling to identify short-circuit pathways to public-supply wells in multiple aquifer settings in the United States. Hydrogeol J 18(3):577–593

Massmann G, Pekdeger A, Merz C (2004) Redox processes in the Oderbruch polder groundwater flow system in Germany. Appl Geochem 19(6):863–886

Massmann G, Nogeitzig A, Taute T, Pekdeger A (2008a) Seasonal and spatial distribution of redox zones during lake bank filtration in Berlin, Germany. Environ Geol 54(1):53–65

Massmann G, Sültenfuß J, Dünnbier U, Knappe A, Taute T, Pekdeger A (2008b) Investigation of groundwater residence times during bank filtration in Berlin: a multi-tracer approach. Hydrol Process 22:788–801. https://doi.org/10.1002/hyp.6649

Neuman SP (1974) Effect of partial penetration on flow in unconfined aquifers considering delayed gravity response. Water Resour Res 10(2):303–312

Omar MEDM, Moussa AMA (2016) Water management in Egypt for facing the future challenges. J Adv Res 7(3):403–412. https://doi.org/10.1016/j.jare.2016.02.005

Paufler S (2015) Management of riverbank filtration sites to reduce manganese concentrations in raw water. Diploma thesis, HTW Dresden, Division of Water Sciences, 157p (**in German**)

Pholkern K, Srisuk K, Grischek T, Soares M, Schäfer S, Archwichai L, Saraphirom P, Pavelic P, Wirojanagud W (2015) Riverbed clogging experiments at potential river bank filtration sites along the Ping River, Chiang Mai, Thailand. Environ Earth Sci 73(12):7699–7709

Przybyłek J, Dragon K, Kaczmarek PMJ (2017) Hydrogeological investigations of river bed clogging at a river bank filtration site along the River Warta, Poland. Geologos 23(3):201–214. https://doi.org/10.1515/logos-2017-0021

Ray C, Melin G, Linsky RB (2003) Riverbank filtration—improving source water quality. Kluwer, Dordrecht, p 364

Regnery J, Barringer J, Wing AD, Hoppe-Jones C, Teerlink J, Drewes JE (2015) Start-up performance of a full-scale riverbank filtration site regarding removal of DOC, nutrients, and trace organic chemicals. Chemosphere 127:136–142

Sandhu C, Grischek T, Kumar P, Ray C (2011) Potential for riverbank filtration in India. Clean Technol Environ Policy 13(2):295–316

Schubert J (2002) Hydraulic aspects of riverbank filtration-field studies. J Hydrol 266(3–4):145–161. https://doi.org/10.1016/S0022-1694(02)00159-2

Sefelnasr A, Sherif M (2014) Impacts of seawater rise on seawater intrusion in the Nile delta aquifer, Egypt. Groundwater 52(2):264–276

Sengupta AK, Shi B (1992) Selective alum recovery from clarifier sludge. J Am Water Works Assoc 84(1):96–104

Sherif MM (1999) The Nile Delta aquifer in Egypt. In: Bear (ed) Seawater intrusion in coastal aquifers: concepts, methods and practices. Theory and application of transport in porous media, vol 14. Kluwer, Dordrecht, pp 559–590

Su GW, Jasperse J, Seymour D, Constantz J (2004) Estimation of hydraulic conductivity in an alluvial system using temperatures. Ground Water 42:890–901. https://doi.org/10.1111/j.1745-6584.2004.t01-7-x

Sukop MC (2000) Estimation of vertical concentration profiles from existing wells. Ground Water 38(6):836–841. https://doi.org/10.1111/j.1745-6584.2000.tb00681.x

Suratman S, Zakaria MP, Samuding K (2014) Groundwater and surface-water utilization using a bank infiltration technique in Malaysia. Hydrogeol J 22(3):543–564

Tügel F, Houben G, Graf T (2016) How appropriate is the Thiem equation for describing groundwater flow to actual wells? Hydrogeol J 24(8):2093–2101. https://doi.org/10.1007/s10040-016-1457-0

Ulrich C, Hubbard SS, Florsheim J, Rosenberry D, Borglin S, Trotta M, Seymour D (2015) Riverbed clogging associated with a California Riverbank filtration system: an assessment of mechanisms and monitoring approaches. J Hydrol 529(3):1740–1753. https://doi.org/10.1016/j.jhydrol.2015.08.012

von Gunten HR, Karametaxas G, Keil R (1994) Chemical processes in infiltrated riverbed sediments. Environ Sci Technol 28(12):2087–2093. https://doi.org/10.1021/es00061a017

Winston RB (2009) ModelMuse—a graphical user interface for MODFLOW-2005 and PHAST. U.S. Geological Survey Techniques and Methods 6-A29, 52p

WWAP (2016) United Nations World Water Assessment Programme. The United Nations World Water Development Report 2016: Water and Jobs. Paris, UNESCO, 164p